Rare Metal Materials and Engineering
Volume 50, Issue 2, February 2021
Available online at www.rmme.ac.cn

Science Press

Cite this article as: Rare Metal Materials and Engineering, 2021, 50(2): 0458-0468.

ARTICLE

Effect of Hydrogen on the Very High Cycle Fatigue Properties of Quenched and Tempered Steels Containing (Ti,Mo)C Precipitates

Jin Xiaokun[1,2], Xu Le[1], Yu Wenchao[1], Yao Kefu[2], Shi Jie[1], Wang Maoqiu[1]

[1] Institute for Special Steels, Central Iron and Steel Research Institute (CISRI), Beijing 100081, China; [2] School of Material Science and Engineering, Tsinghua University, Beijing 100084, China

Abstract: The effects of hydrogen trapping behavior of undissolved and temper-induced (Ti,Mo)C precipitates on the very high cycle fatigue properties of quenched and tempered Cr-Mo steel were investigated. Results reveal that spherical undissolved (Ti,Mo)C precipitates with a hydrogen desorption activation energy of 142.6 kJ/mol cannot trap hydrogen through electrochemical charging; fine, temper-induced (Ti,Mo)C precipitates are effective hydrogen trap sites. Hydrogen trapped by fine, temper-induced (Ti,Mo)C precipitates with a desorption activation energy of 17.0 kJ/mol cannot diffuse out from the sample even if exposed to atmosphere for 336 h, while it may desorb from the trap site under cyclic loading and then diffuse to the crack tip or stress concentration field, resulting in a decrease in fatigue strength. Diffusible hydrogen trapped by dislocations and grain boundaries with a desorption activation energy of 16.9 kJ/mol can rapidly diffuse to crack tip or stress concentration field and then reduce the threshold value of stress intensity factor (SIF) of crack growth remarkably, resulting in a decrease of fatigue strength; this portion of hydrogen can diffuse out from the sample after atmosphere exposure for 96 h; Considering that the hydrogen content in both hydrogen trapping site is equivalent, the deleterious effect of hydrogen trapped by fine, temper-induced (Ti,Mo)C precipitates on fatigue strength is relatively smaller than that of the diffusible hydrogen trapped by dislocations and grain boundaries. Non-metallic inclusions (Al_2O_3) with a hydrogen desorption activation energy of 70.9 kJ/mol also cannot trap hydrogen through electrochemical charging.

Key words: high-strength steel; very high cycle fatigue; hydrogen; (Ti,Mo)C

Quenched and tempered medium carbon Cr-Mo steels are often used as critical structure components in many industries due to their high strength, excellent plasticity and toughness[1]. With the development of modern industries, materials are required to have better performance, higher strength and better fatigue resistance. In many industries, such as high speed train, many structural components are subjected to fatigue loading with a number of cycles higher than 10^7, which is known as very high cycle fatigue (VHCF)[2]. Researches on the VHCF focus mainly on the nature and related mechanisms of the characteristic region of crack initiation, because it consumes more than 90%, even 99% of total fatigue life[3]. This characteristic region was called as optical dark area (ODA) by Murakami et al[4], granular bright facet (GBF) by Shiozawa et al[5], fine granular area (FGA) by Sakai et al[6], or rough surface area (RSA) by Ochi et al[7]. For convenience, GBF was adopted in this research. Hydrogen embrittlement (HE) is also one of the main failure modes of these high strength steels. HE is caused by diffusible hydrogen which can diffuse easily in the lattice at room temperature and accumulate in the stress concentration region. To reduce the HE susceptibility, strong carbide-forming elements such as titanium have been introduced into these high strength steels to form deep hydrogen trapping sites to fix diffusible hydrogen[8]. In fact, it

Received date: February 20, 2020
Foundation item: National Key Research and Development Program (2017YFB0304802, 2016YFB0300102, 2016YFB0300104)
Corresponding author: Jin Xiaokun, Candidate for Ph. D., Institute for Special Steels, Central Iron and Steel Research Institute (CISRI), Beijing 100081, P. R. China, Tel: 0086-10-62186791, E-mail: 2545835925@qq.com

has been reported that titanium carbides can effectively trap hydrogen and improve HE resistance of high strength steels under the static loading with monotonic stress[9-11]. It is also reported that fatigue crack growth rate is accelerated by diffusible hydrogen[12], and fatigue life and fatigue strength decrease considerably with the presence of diffusible hydrogen[13,14]. Murakami et al[4] pro- posed that the formation of GBF might be caused by cyclic stress coupled with internal hydrogen trapped by inclusions. Thus, it is also expected that strong carbides can also act as deep hydrogen trapping sites under cyclic loading and then improve the fatigue properties of high strength steels in the presence of hydrogen. Although the influence of hydrogen trapped by carbides, such as cementite [15] and V-rich MC carbides [16] on fatigue properties have been studied, they have seldom been clarified, and the effect of (Ti,Mo)C carbides on the VHCF properties of high strength martensitic steels in the presence of hydrogen is rarely reported.

In the present study, the effects of hydrogen trapping behavior of undissolved and temper-induced (Ti,Mo)C precipitates on the VHCF properties of quenched and tempered low alloy Cr-Mo steel were investigated, and the deleterious effect of hydrogen trapped by temper-induced (Ti,Mo)C precipitates on the VHCF properties was confirmed.

1 Experiment

1.1 Materials and heat treatment

The material used was a commercial Cr-Mo low alloy steel micro-alloyed with Ti. The as-received steel was hot rolled into wire rod with a diameter of 12 mm and its chemical composition is listed in Table 1. Round rods with suitable length were machined from the as-received steel in the longitudinal direction, austenitized at 880 °C for 15 min and oil quenched, and then tempered at different temperatures for 2 h, followed by air cooling. To fully dissolve precipitates during austenitizing, an austenitizing temperature of 1350 °C was selected.

1.2 Microstructural characterization and Mechanical evaluation

After heat treatment, standard tensile samples (Φ5 mm, parallel length of 30 mm) were tested at room temperature using a WE-300 machine according to Chinese national standard GB/T 228.1-2010. According to the variations of ultimate tensile strength with tempering temperature shown in Fig.1, and the microstructures of the experimental steels, two kinds of samples with a similar tensile strength of 1300 MPa were selected and signified as 880-450 and 1350-550 samples, where the numbers indicate the austenitizing temperature and tempering temperature, respectively, to study the hydrogen trapping behavior of titanium carbide and its effect on the VHCF properties of high strength steels. The metallographic samples for scanning electron microscope (SEM, Hitachi S-4300) observation were ground, mechanically polished and etched in 4% nital solution for 10 s. Due to the strong magnetism, carbon extraction replicas were used for HR-TEM (JEM-2100F) observation and analyzed by energy dispersive spectrometer (EDS) and selected area electron diffraction (SAED). Carbon extraction replicas were prepared by plating a carbon film with a thickness of 20~30 nm on the sample surface etched with 4% nital after mechanical polishing. Then, the carbon films were extracted with 4% nital and taken out with a copper net. Chemical extraction phase analysis was also used to analyze the precipitates according to ISO/ TS13762 standard.

Table 1 Chemical compositions of the experimental steel (wt%)

C	Si	Mn	S	P	Cr	Mo	Ti	Fe
0.30	0.15	0.31	0.002	0.006	1.36	0.18	0.08	Bal.

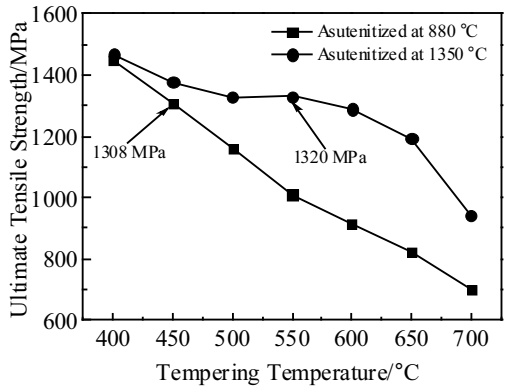

Fig.1 Variation of ultimate tensile strength with tempering temperature

1.3 Thermal desorption spectroscopy (TDS) analysis

Hydrogen was introduced into the materials by electro-chemical charging using 0.1 mol/L NaOH aqueous solution at room temperature. Cylindrical samples with a diameter of 5 mm and a length of 25 mm were charged for 72 h at a current density of 1.2 mA/cm^2. After hydrogen charging, parts of the hydrogen charged specimens were exposed to atmosphere for different time (12~336 h) to study the hydrogen trapping and desorption behavior. TDS analysis was performed to deter-mine the hydrogen contents and locations. The heating rate was 100 K/h. The hydrogen desorption curves can be obtained through fitting the residual hydrogen content vs atmosphere exposure time curves. The hydrogen desorption activation energy for the samples can be calculated according to the Choo-Lee equation[17]:

$$\frac{\partial \ln(\varphi/T_c^2)}{\partial(1/T_c)} = -E_a/R \quad (1)$$

where E_a is the hydrogen desorption activation energy (kJ/mol), φ is the heating rate (K/h), T_c is the peak temperature, and R is the gas constant. If φ and T_c are known, E_a can be easily calculated from the slope of a $\partial \ln(\varphi/T_c^2)$ vs $1/T_c$ plot. In this study, heating rates of 100, 200, 300 and 400 K/h were used to calculate the hydrogen desorption activation energy. For simplicity, the hydrogen uncharged, hydrogen charged and hydrogen charged and atmosphere exposed samples were termed as HF, HC and HCAE samples, respectively.

1.4 Fatigue testing

Tension-compression fatigue tests with a load ratio of −1 were carried out on a Shimadzu USF-2000 ultrasonic fatigue testing system in laboratory air at room temperature. The resonance frequency was 20 kHz. Fatigue tests were conducted up to 1×10^9 cycles and the fatigue strength was figured out by the stress up and down method through at least six pairs in order to improve the accuracy. During the tests, compressive air was used to cool the specimens. An intermittent loading (150 ms of pulse and 150 ms of pause) was employed to further reduce the thermal effect. So the time required to reach 1×10^9 cycles was 28 h. According to the hydrogen desorption curves at room temperature described in Section 1.3, this interval was acceptable to obtain the fatigue strength up to 1×10^9 cycles before the specimens lose most of hydrogen. Smooth hour-glass type specimen was used for fatigue testing. The geometry and dimensions of the specimen are shown in Fig.2. The length of the specimen's shoulder was calculated to be 10.46 mm, which is dependent on the Yong's modulus and density. After fatigue tests, the fracture surfaces of all failed fatigue specimens were observed using SEM (FEI, Quanta 650FEG), operated at 25 kV.

2 Results and Discussion

2.1 Microstructural characterization

The samples of 880-450 and 1350-550 exhibit a typical tempered martensitic microstructure, as shown in Fig.3a and Fig.3b, respectively. The microstructure of 1350-550 is clearly coarser than that of the 880-450 sample due to the higher austenitizing temperature.

Chemical extraction phase analysis results (Table 2) show that nearly all the titanium forms (Ti,Mo)C precipitates in the as-received hot-rolled wire rod (880-Q means that the sample is quenched at 880 °C). Small-angle scattering results show that these (Ti,Mo)C particles are mainly in the range of 36~60 nm. According to the solid solubility product formula[18]:

$$\lg[\mathrm{Ti}][\mathrm{C}] = -\frac{7000}{T} + 2.75 \quad (2)$$

when the quenching temperature is 880 °C, the (Ti,Mo)C particles formed during hot rolling will not dissolve in austenite. Thus, no new (Ti,Mo)C particles will be precipitated during the subsequent tempering process. These (Ti,Mo)C precipitates formed during hot rolling will be retained in the 880-450 sample. HR-TEM results (Fig.4) show that (Ti,Mo)C particles with 40~60 nm in diameter are found in the 880-450 sample, which is consistent with the chemical extraction phase analysis result. As shown in Fig.4a, the embedded figure shows the SAED pattern of (Ti,Mo)C particles. When the austenitizing temperature is 1350 °C, nearly all the (Ti,Mo)C particles may re-dissolve in austenite, according to the solid solubility product in Eq.(2). Fine (Ti,Mo)C particles can precipitate during tempering at 550 °C after 1350 °C austenitizing, resulting in a secondary hardening platform around 550 °C, as can be seen in Fig.1. Wei et al[19] found that 0.42C-0.30Ti

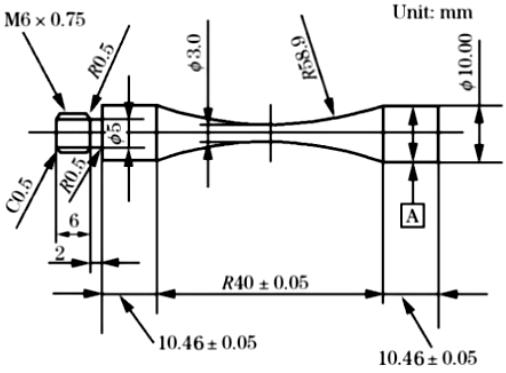

Fig.2 Dimensions of the specimen used in the VHCF testing

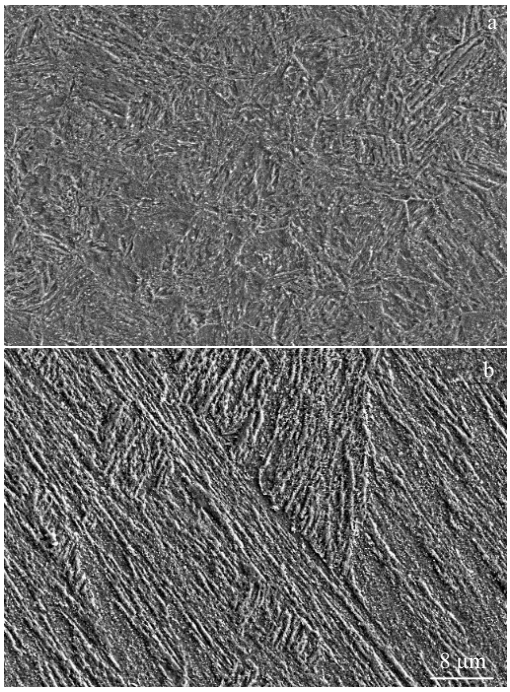

Fig.3 SEM images of samples: (a) 880-450 and (b) 1350-550

Table 2 Element contents of the *M*C phase in the specimen (wt%)

Sample	Ti	Mo	N	C	Total
As-received	0.078	0.027	0.0047	0.019	0.129
880-Q	0.076	0.024	0.0049	0.018	0.123
880-450	0.074	0.024	0.0048	0.017	0.120
1350-Q	0.034	0.003	0.0045	0.005	0.047
1350-550	0.055	0.024	0.0047	0.013	0.097

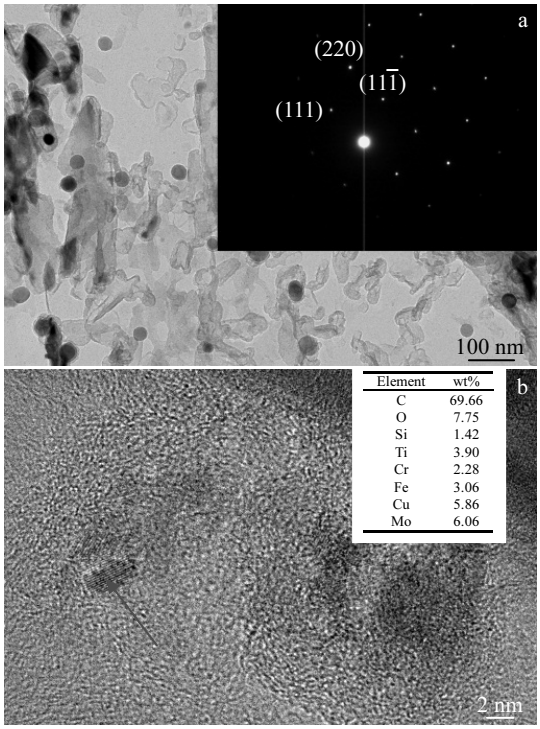

Fig.4 HR-TEM images and SAED pattern of 880-450 sample showing spherical undissolved (Ti,Mo)C particles (a) and fine temper-induced (Ti,Mo)C particles and EDS results (b)

steel also exhibited a secondary hardening peak at 550 °C when quenched at 1350 °C. Fawakhry et al[20] also reported that adding titanium can increase the tempering resistance in the early stages of tempering and cause secondary hardening at 550~600 °C. HR-TEM morphology of the fine tempered (Ti,Mo)C particle is shown in Fig.4b, where the embedded figure shows the EDS results of (Ti,Mo)C particles. The chemical extraction phase analysis results (Table 2, 1350-Q means that the sample is quenched at 1350 °C) also indicate that fine particles are found in the 1350-550 sample, which consists mainly of Ti, Mo, and C. Small angle scattering result indicates that these newly precipitated (Ti,Mo)C particles are mainly in the size range of 1~5 nm, which is consistent with the HR-TEM result.

2.2 Hydrogen trapping and desorption behavior

TDS curves of the HF, HC and HCAE samples are shown in Fig.5a and Fig.5b. Fig.5c and Fig.5d show the locally enlarged views of TDS curves from 300 °C to 600 °C of HF and HC samples. At a heating rate of 100 °C/h, for the uncharged specimens, 880-450 specimens show two small hydrogen desorption peaks at 363 °C (called peak 2) and 519 °C (called peak 3). 1350-550 specimens only show peak 2 but no peak 3. There is no significant difference for peak 2 and peak 3 between hydrogen charged and uncharged specimens. Compared to the HF specimens, HC specimens show additional hydrogen desorption peak at a lower temperature (called peak 1). Clearly, electrochemical charging at room temperature does not influence the two high-temperature hydrogen desorption peaks (peak 2 and peak 3) but is directly responsible for the appearance of the low-temperature peak (peak 1). As shown in Fig.5a and Fig.5b, the height of peak 1 decreases with increasing the exposing time, indicating that hydrogen content decreases with prolonging the exposing time. As shown in Fig.6 and Table 3, nearly all the hydrogen has already diffused out from the 880-450 samples after atmosphere exposing for 96 h. However, there are still 1.85 μg/g hydrogen in the 1350-550 samples after atmosphere exposing for 96 h, as shown in Fig.5b and Table 3, and hydrogen content does not decrease significantly even after exposure for 336 h, as shown in Fig.5b.

Many microstructures or defects may be hydrogen trapping sites in the steel, such as grain boundaries, dislocations, nonmetallic inclusions and carbides. Different trapping sites can be determined by calculating the hydrogen desorption activation energy, as described in Section 1.3. Plot of $\ln(\varphi/T_p^2)$ vs $1/T_p$ for determining the hydrogen desorption activation energy of each peak observed in 880-450 sample is shown in Fig.7a. As demonstrated in Fig.7a, the values of hydrogen desorption activation energy corresponding to peak 1, peak 2, and peak 3 obtained for pre-charged 880-450 steel are 16.9, 70.9 and 142.6 kJ/mol, respectively. From the hydrogen desorption activation energy, the hydrogen introduced into 880-450 steel through electrochemical charging corresponding to peak 1 should be the hydrogen trapped by dislocation and

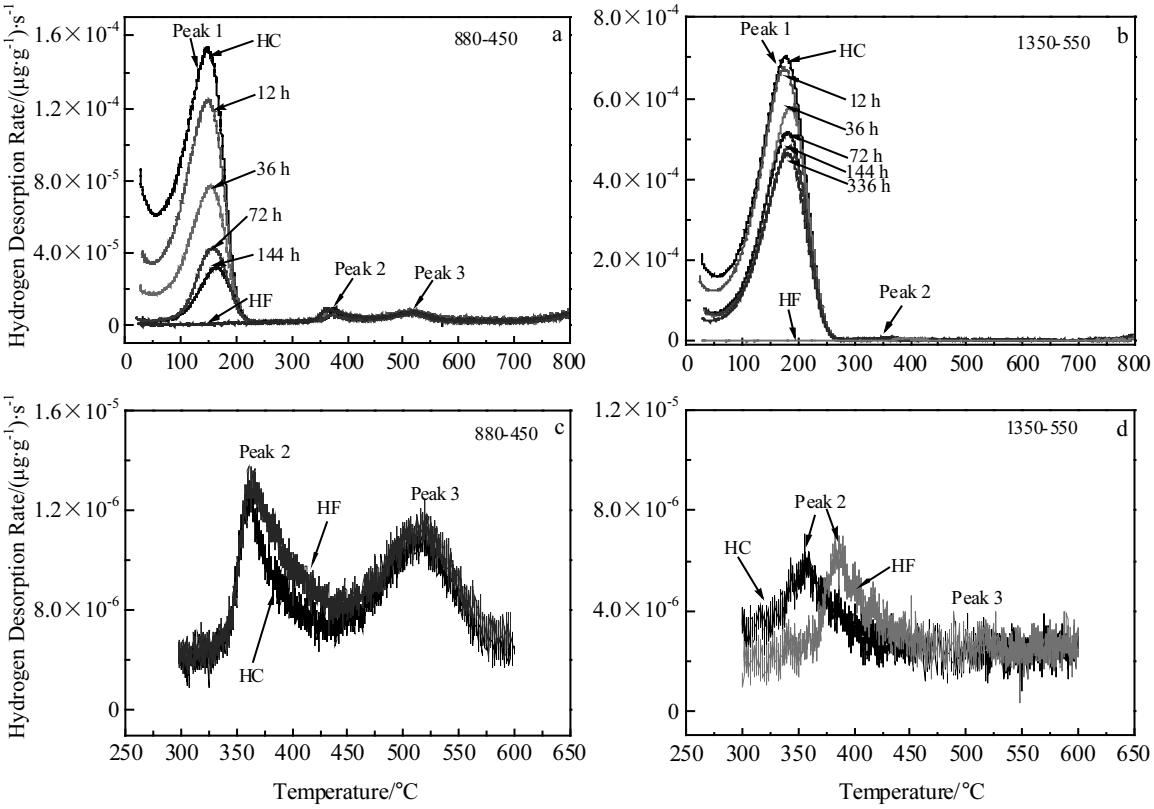

Fig.5 TDS curves of HF, HC and HCAE specimens of 880-450 (a) and 1350-550 (b); locally amplified TDS curves of HF and HC specimens of 880-450 (c) and 1350-550 (d) at 300~600 °C

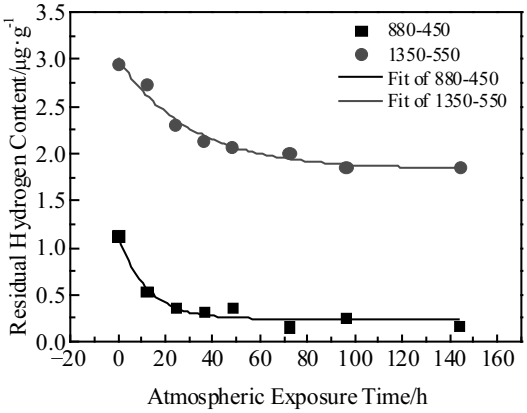

Fig.6 Variation of total hydrogen content with atmospheric exposure time

prior austenite grain boundaries[21-24]; peak 2 should correspond to the hydrogen trapped in the interface of nonmetallic inclusions of Al_2O_3 and matrix[25]; peak3 observed in the 880-450 sample should correspond to the hydrogen trapped by undissolved (Ti,Mo)C incoherent interface[26]. Both Hui[16] and Li et al[27] reported that cathodic charging does not change the hydrogen trapped by inclusions. Wei et al[28] and Turnbull[29] reported that the energy barrier for hydrogen to jump into incoherent TiC is too high at low temperatures so incoherent TiC will not trap hydrogen through electrochemical charging at room temperature. Hence, as shown in Fig.5c, nonmetallic inclusions of Al_2O_3 and the undissolved (Ti,Mo)C interface cannot absorb hydrogen through electrochemical hydrogen charging at room temperature.

When the austenitizing temperature is 1350 °C, nearly all the undissolved (Ti,Mo)C is redissolved into austenite. Hence, peak 3 disappears in 1350-550 samples. As previously stated,

Table 3 Hydrogen content for different samples under different conditions (μg/g)

Sample	Uncharged	1.2 mA/cm^2-72 h, exposure-0 h	1.2 mA/cm^2-72 h, exposure-96 h
880-450	0.09	1.12	0.26
1350-550	0.06	2.97	1.85

the microstructures of 880-450 and 1350-500 steels are tempered martensite, and the essential differences between the two steels are the undissolved and newly precipitated fine, temper-induced (Ti,Mo)C particles. When hydrogen is charged and exposed to atmosphere for 96 h, reversible hydrogen trapped by grain boundaries and dislocations in 880-450 samples will diffused out from the samples, while there is still 1.85 μg/g hydrogen in the 1350-550 samples. This strongly indicates that this part of hydrogen is trapped by these fine, temper-induced (Ti,Mo)C particles. As shown in Fig.7b, the desorption activation energy of this part of hydrogen is calculated to be 17.0 kJ/mol.

2.3 Fatigue properties

Fig.8 shows the *S-N* curves of all the experiment specimens. The fatigue strength is listed in Table 4. It is clear that the HF 880-450 and 1350-550 samples have similar fatigue strength and fatigue strength ratio σ_w/R_m due to the similar strength. After hydrogen charging at the same current density, approximately 1.12 and 2.97 μg/g total hydrogen are introduced into 880-450 and 1350-550 specimens, respectively, and both the fatigue strength and fatigue strength ratio of the two samples decrease significantly, which is about 22% and 24% for the 880-450 and 1350-550 samples, respectively. After hydrogen charging and atmosphere exposing for 96 h, approximately 1.12 μg/g reversible hydrogen trapped by dislocations and grain boundaries diffuses out from the 1350-550 specimen and 1.85 μg/g hydrogen trapped by fine, temper-induced (Ti,Mo)C particles still exists in the specimens and the fatigue strength and the fatigue strength ratio of 1350-550 specimens are recovered to a large extent. However, the fatigue strength of HCAE 1350-550 specimen is still 7% lower, approximately 44 MPa, than that of the HF 1350-550 specimen. Nearly all the hydrogen diffuses out from the 880-450 sample after exposing to atmosphere for 96 h, so the

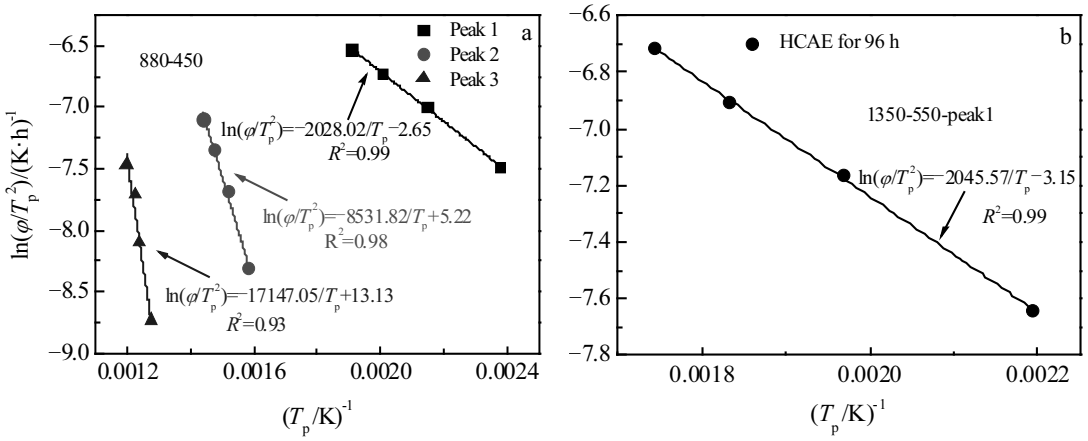

Fig.7 Plots of $\ln(\varphi/T_p^2)$ vs $1/T_p$ for determining the hydrogen trapping activation energy of 880-450 (a) and 1350-550 (b) steels

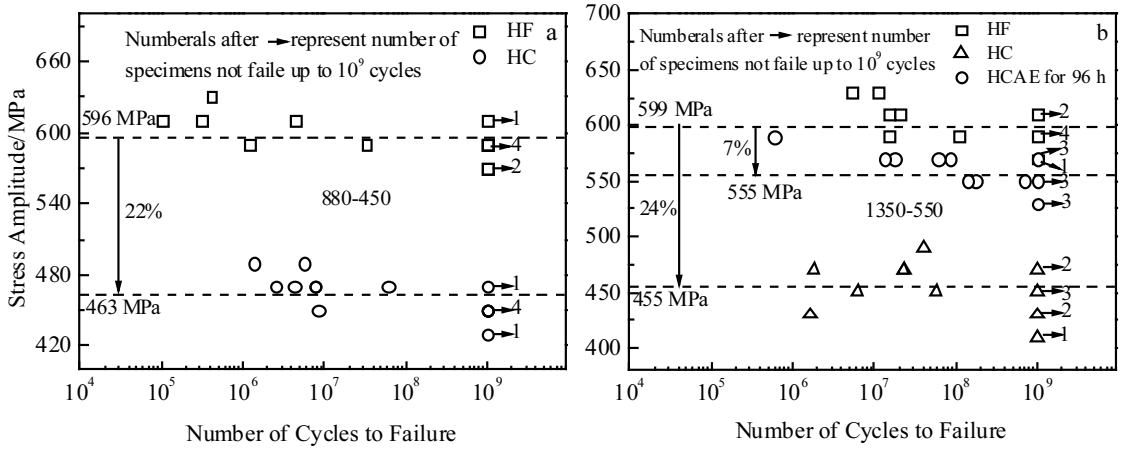

Fig.8 *S-N* curves of HF and HC 880-450 specimens (a) and HF, HC and HCAE 1350-550 specimens (b)

Table 4 Summary of tensile strength and fatigue strength of the tested steels

Specimen	Tensile strength, R_m/MPa	Fatigue strength, σ_w/MPa	σ_w/R_m
HF 880-450	1308	596	0.46
HC 880-450		463	0.35
HF 1350-550	1320	599	0.45
HC 1350-550		455	0.34
HCAE 1350-550		555	0.42

fatigue strength should be fully recovered.

2.4 Fatigue fracture surface

All the fatigue fracture surface was analyzed by SEM. Fatigue fracture initiation sites and inclusion types at fatigue fracture origins are listed in Table 5. It seems that cracks are more likely to occur at surface inclusions for HF 880-450 and 1350-550 specimens due to their higher percentage in all the different initiation modes, which is 66.7% and 50% for 880-450 and 1350-550 HF specimens. However, after hydrogen charging, the fatigue fracture initiation sites all transform to internal inclusions for the HC 880-450 and 1350-550 specimen, indicating that fatigue fracture mode is changed by hydrogen. After hydrogen charging and atmosphere exposing for 96 h, fatigue fracture initiation sites are still internal, with 50% internal inclusions and 50% internal matrix, and no surface initiation sites are observed for the HCAE 1350-550 specimens. The inclusions at fracture origins are Al_2O_3·MgO and Al_2O_3·CaO or their composites.

Typical SEM micrographs of fatigue fracture surfaces with different fatigue fracture initiation modes of 880-450 and 1350-550 specimens are shown in Fig.9 and Fig.10. It is observed that there is a GBF feature in specimen with long life (generally>10^7 cycles), although Hui et al[30] recently reported that hydrogen charged specimens are more prone to form GBF feature even in the short life (10^4 and 10^5 cycles) regions.

2.5 Effect of hydrogen on GBF

As already mentioned in the introduction, GBF is the characteristic region for VHCF. As shown in Table 6, the SIF range of GBFs, ΔK_{GBF} of the experimental steels with obvious GBF feature before and after hydrogen charging can be calculated by the Murakami's formula[31]:

$$\Delta K_{GBF} = 0.5\Delta\sigma_a\sqrt{\pi\sqrt{\text{area}_{GBF}}} \quad (3)$$

where ΔK_{GBF} is the SIF range of GBFs (MPa·$m^{1/2}$); $\Delta\sigma_a$ is the applied stress amplitude (MPa); $\sqrt{\text{area}_{GBF}}$ is the square root of the projective area of GBFs (m). The traditional crack growth threshold (ΔK_{th}), a threshold SIF value below which the existing crack will stop propagating, derived by Weertman[32] is expressed as:

$$\Delta K_{th} \approx 2E\sqrt{\frac{2b}{5}} \approx 3.289\mu\sqrt{b} \quad (4)$$

where b is Burgers vector; μ is shear modulus. For steels, b≈0.25 nm, μ≈81 GPa, so the calculated threshold value $\Delta K_{th} \approx 4.200\ \text{MPa}\cdot\text{m}^{1/2}$, which is very close to the calculated ΔK_{GBF} values of HF 880-450 and HF 1350-550 samples, and this is why the ΔK_{GBF} is generally considered as the effective SIF of crack to start propagate. From Weertman model, it is seen that the threshold value only depends on the Burgers vector and shear modulus of materials, so the calculated ΔK_{GBF} value of HF 880-450 and HF 1350-550 samples is almost the same, irrelevant to different tempering treatments. However, as shown in Table 6, after hydrogen charging, the ΔK_{GBF} of HC 880-450 and HC 1350-550 samples decreases obviously. TDS results show that hydrogen trapped by inclusion does not increase remarkably after hydrogen charging

Table 5 Summary of fatigue fracture initiation sites and inclusion types at fatigue fracture origins

Specimen	Total number of fatigue specimens	Number of fatigue specimens with different initiation modes			Inclusion types
		Surface inclusion	Internal inclusion	Internal matrix	
HF 880-450	6	4	2	0	Al_2O_3·MgO·CaO
HC 880-450	7	0	7	0	
HF 1350-550	6	3	1	2	
HC 1350-550	6	0	6	0	
HCAE 1350-550	8	0	4	4	

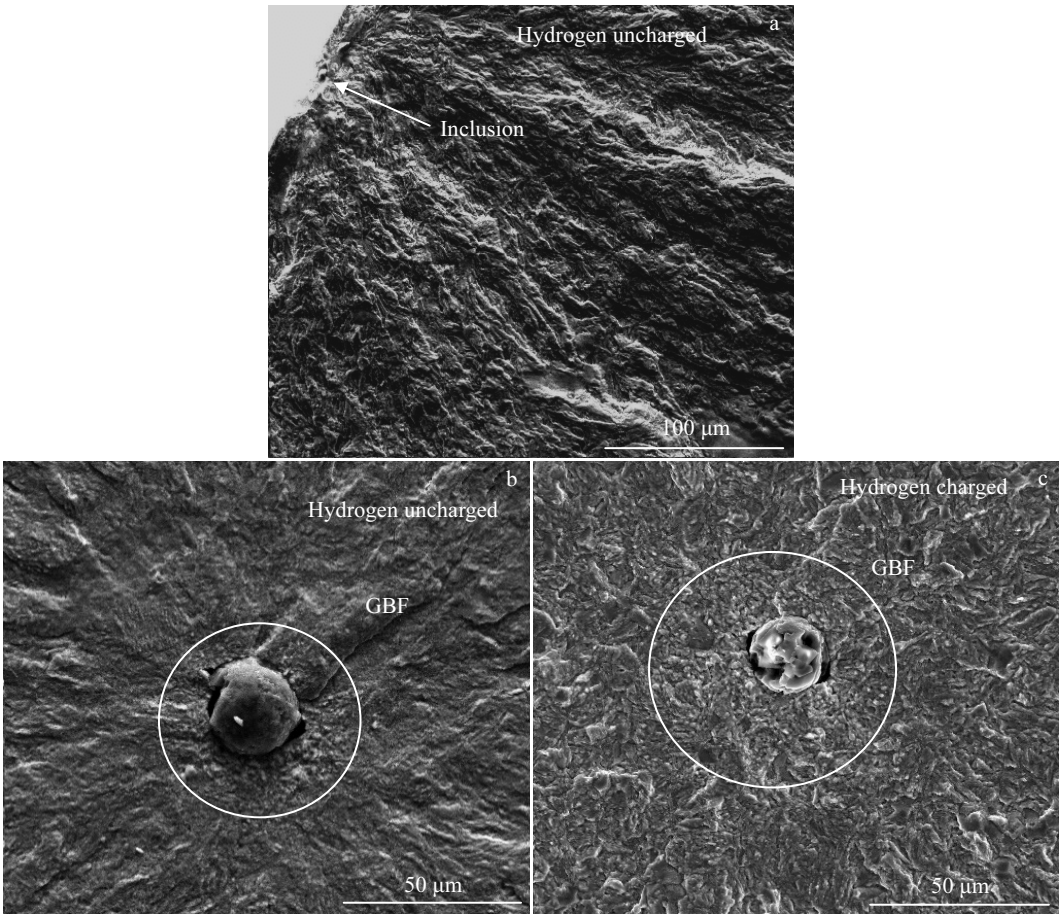

Fig.9 SEM morphologies of fatigue fracture surfaces of HF (a, b) and HC (c) 880-450 samples with different crack initiation origins: (a) surface inclusion, σ_a=590 MPa, N_f =1.236×10^6 cycles; (b) internal inclusion and its surrounding area (GBF), σ_a=590 MPa, N_f =3.273×10^7 cycles; (c) internal inclusion and its surrounding area (GBF), σ_a=470 MPa, N_f =5.983×10^7 cycles

(Fig.5c) so the detrimental influence of introduced hydrogen on fatigue properties should be attributed to diffusible hydrogen trapped by reversible trapping sites such as dislocations and grain boundaries. These diffusible hydrogen has a higher diffusion coefficient, and it is easy to accumulate at the stress concentration area and the inclusion interface under the cycle loading and decrease the threshold SIF values, so the fatigue fracture may occur under a lower stress and the fatigue fracture initiation sites transform to internal inclusions after hydrogen charging. After hydrogen charging and exposing to atmosphere for 96 h, nearly all the hydrogen has diffused out from the 880-450 sample, so it is conceivable that the VHCF strength of 880-450 samples should also recover.

After exposing to atmosphere for 96 h, nearly all the diffusible hydrogen, approximately 1.12 μg/g in the 1350-550 sample is diffused out from the sample and 1.85μg/g hydrogen is still trapped by temper-induced (Ti,Mo)C. This portion of hydrogen is uniformly distributed in the matrix with (Ti,Mo)C precipitates and does not diffuse easily, as shown in Fig.5b and Fig.6. Nakatani et al[33,34] confirmed that the irreversible hydrogen with a hydrogen desorption activation energy higher than 60 kJ/mol can desorb out from the deep trap site under cyclic loading, and the fatigue strength was decreased by the desorbed irreversible hydrogen through TDS and hydrogen microprint technique. In the present study, the desorption activation energy of hydrogen trapped by temper-induced (Ti,Mo)C was calculated to be 17.0 kJ/mol (Fig.7b). As Nakatani stated, cyclic deformation induces a desorption of hydrogen from temper-induced (Ti,Mo)C; hydrogen desorbs from the trap site then diffuses to the crack tip or stress concentration field, resulting in a decrease in fatigue strength. For the HF 1350-550 sample, both the internal inclusions (Fig.10c) and internal matrix such as grain boundaries (Fig.10b) can act as fatigue crack initiation sites, so the desorbed hydrogen from temper-induced (Ti,Mo)C can diffuse to inclusion interface or grain boundaries and decrease the

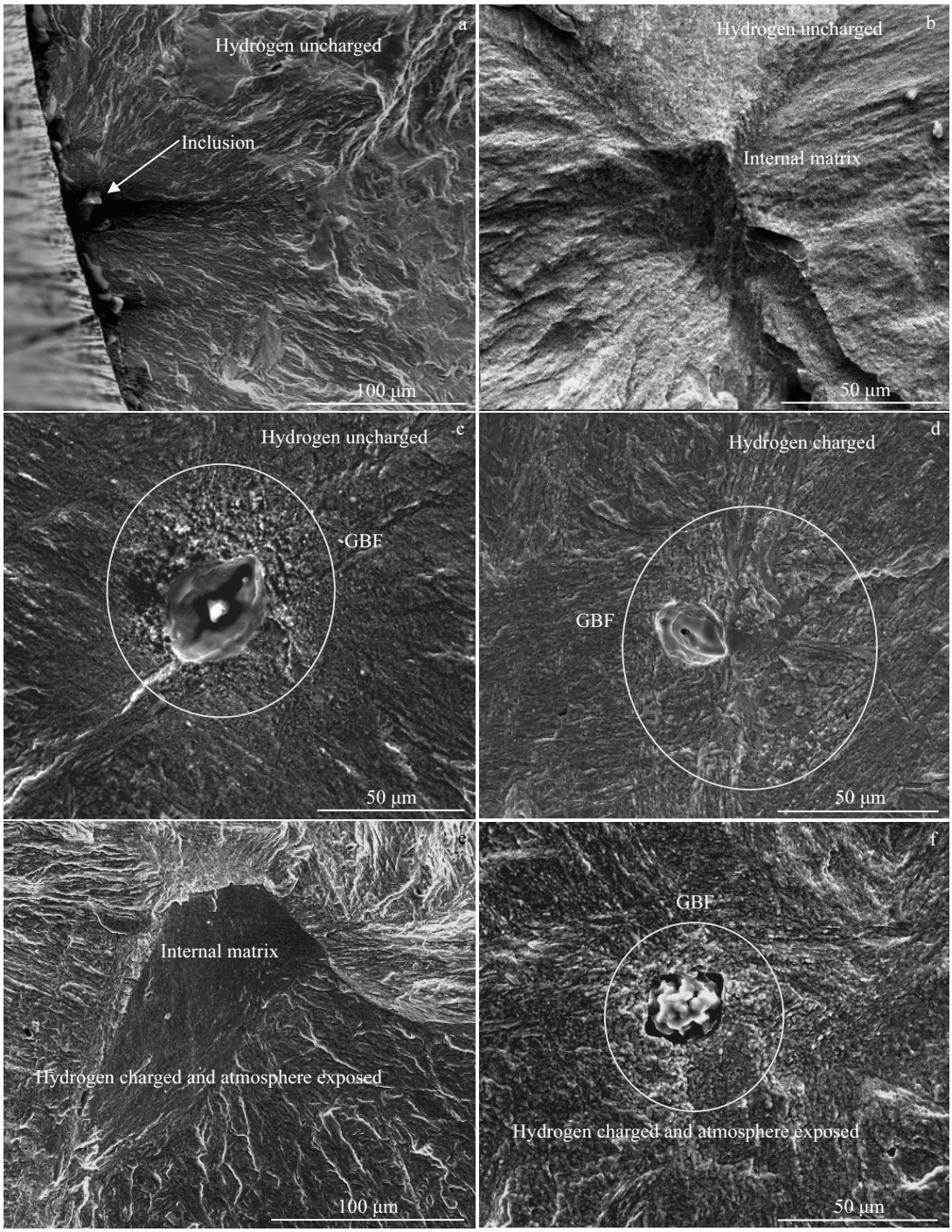

Fig.10 SEM morphologies of fatigue fracture surfaces of HF (a~c), HC (d) and HCAE (e, f) 1350-550 samples with different crack initiation origins: (a) surface inclusion, σ_a= 610 MPa, N_f=2.101×10^7 cycles; (b) internal matrix, σ_a=610 MPa, N_f =1.49×10^7 cycles; (c) internal inclusion and its surrounding area (GBF), σ_a=590 MPa, N_f=1.088×10^8 cycles; (d) internal inclusion and its surrounding area (GBF), σ_a=450 MPa, N_f=5.711×10^7 cycles; (e) internal matrix, σ_a=570 MPa, N_f=1.355×10^7 cycles; (f) internal inclusion and its surrounding area (GBF), σ_a=550 MPa, N_f=1.382×10^8 cycles

threshold SIF values, and thus the fatigue fracture occurs under a lower stress. The deleterious effect of hydrogen trapped by temper-induced (Ti,Mo)C is relatively small compared to the diffusible hydrogen trapped by dislocations and grain boundaries, considering that the hydrogen content in the both hydrogen trapping site is equivalent.

Table 6 Inclusion information for calculation of ΔK_{GBF}

Specimen	$\sqrt{area}_{inc}$ /μm	$\sqrt{area}_{GBF}$ /μm	σ_a/MPa	N_f/×10^7 cycles	ΔK_{GBF}/MPa·m $^{1/2}$
HF 880-450	27.98	62.85	610	0.4345	4.29
	25.42	58.84	590	3.273	4.01
HC 880-450	21.48	60.14	470	5.983	3.23
	17.21	44.84	510	3.443	3.03
HF 1350-550	30.26	71.58	590	10.88	4.42
HC 1350-550	18.35	74.80	450	5.711	3.45
HCAE 1350-550	28.83	57.89	570	6.135	3.84
	21.06	66.40	550	13.82	3.97

3 Conclusions

1) Hydrogen trapped by non-metallic inclusion with a desorption activation energy of 70.9 kJ/mol will not increase remarkably, so the deleterious effect of introduced hydrogen through electrochemical charging on fatigue strength should not be attributed to hydrogen trapped by non-metallic inclusions.

2) Diffusible hydrogen trapped by dislocations and grain boundaries with a desorption activation energy of 16.9 kJ/mol can rapidly diffuse to crack tip or stress concentration field and then reduce the threshold value of SIF of crack growth remarkably, resulting in a decrease of fatigue strength.

3) Spherical undissolved (Ti,Mo)C particles with a desorption activation energy of 142.6 kJ/mol cannot trap hydrogen through electrochemical charging. Hydrogen trapped by fine, temper-induced (Ti,Mo)C precipitates with a desorption activation energy of 17.0 kJ/mol can desorb from the trap site under cyclic loading and then diffuse to the crack tip or stress concentration field, resulting in a decrease in fatigue strength. However, considering that the hydrogen content in the both hydrogen trapping site is close, the deleterious effect of hydrogen trapped by fine, temper-induced (Ti,Mo) precipitates is relatively smaller than that of the diffusible hydrogen trapped by dislocations and grain boundaries.

References

1 Varun R N. *Dissertation for Doctorate*[D]. Detroit: Wayne State University, 2014

2 Pyttel B, Schwerdt D, Berger C. *International Journal of Fatigue*[J], 2011, 33: 49

3 Li Y D, Zhang L L, Fei Y H *et al*. *International Journal of Fatigue*[J], 2016, 82: 402

4 Murakami Y, Yokoyama N N, Nagata J. *Fatigue & Fracture of Engineering Materials & Structures*[J], 2002, 25: 735

5 Shiozawa K, Lu L, Ishihara S. *Fatigue & Fracture of Engineering Materials & Structures*[J], 2001, 24: 781

6 Sakai T, Sato Y, Oguma N. *Fatigue & Fracture of Engineering Materials & Structures*[J], 2002, 25: 765

7 Ochi Y, Matsumura T, Masaki K *et al*. *Fatigue & Fracture of Engineering Materials & Structures*[J], 2002, 25: 823

8 Takahashi J, Kawakami K, Kobayashi Y *et al*. *Scripta Materialia*[J], 2010, 63: 261

9 Nagao A, Martin M L, Dadfarnia M *et al*. *Acta Materialia*[J], 2014, 74: 244

10 Depover T, Verbeken K. *Corrosion Science*[J], 2016, 112: 308

11 Hui W J, Dong H, Weng Y Q *et al*. *Journal of Iron and Steel Research International*[J], 2005, 12: 43

12 Tazoe T, Hamada S, Noguchi H. *International Journal of Hydrogen Energy*[J], 2017, 42: 13 158

13 Li Y D, Yang Z G, Liu Y B *et al*. *Materials Science and Engineering A*[J], 2008, 489: 373

14 Yang Z G, Li S X, Li Y D *et al*. *Materials Science and Engineering A*[J], 2010, 527: 559

15 Nakatani M, Fujihara H, Sakihara M *et al*. *Materials Science and Engineering A*[J], 2011, 528: 7729

16 Hui W J, Zhang Y J, Zhao X L *et al*. *Materials Science and Engineering A*[J], 2016, 651: 311

17 Choo W Y, Lee J Y. *Metallurgical Transactions A*[J], 1982, 13: 135

18 Lee S M, Lee J Y. *Acta Metallurgica*[J], 1987, 35: 2695

19 Wei F G, Hara T, Tsuchida T *et al*. *ISIJ International*[J], 2003, 43: 539

20 Fawakhry K E, Mishreky M L, Eissa M. *Scandinavian Journal of Metallurgy*[J], 1990, 19: 33

21 Wang M Q, Akiyama E, Tsuzaki K. *Corrosion Science*[J], 2007, 49: 4081

22 Wang M Q, Akiyama E, Tsuzaki K. *Materials Science and Engineering A*[J], 2005, 398: 37

23 Wei F G, Hara T, Tsuzaki K. *Metallurgical and Materials Transactions B*[J], 2004, 35: 587

24 Yamasaki S, Takahashi T. *Tetsu-to-Hagané*[J], 1997, 83: 454

25 Lee J L, Lee J Y. *Metallurgical Transactions A*[J], 1986, 17: 2183

26 Escobar D P, Wallaert E, Duprez L *et al*. *Metals and Materials International*[J], 2013, 19: 741
27 Li Y D, Chen S M, Liu Y B *et al*. *Journal of Materials Science*[J], 2010, 45: 831
28 Wei F G, Tsuzaki K. *Metallurgical and Materials Transactions A*[J], 2004, 35: 3155
29 Turnbull A. *International Journal of Hydrogen Energy*[J], 2015, 40: 16 961
30 Hui W J, Chou C, Zhang Y J *et al*. *Fatigue & Fracture of Engineering Materials & Structures*[J], 2016, 39: 1081
31 Murakami Y, Yamashita Y. *Procedia Engineering*[J], 2014, 74: 6
32 Weertman J. *Applied Mechanics Division, AMD*[J], 1981, 47: 11
33 Nakatani M, Fujihara H, Sakihara M *et al*. *Materials Science and Engineering A*[J], 2011, 528: 7729
34 Nakatani M, Minoshima K. *Fatigue & Fracture of Engineering Materials & Structures*[J], 2010, 34: 363

氢对含(Ti,Mo)C 析出相的调质钢的超高周疲劳性能的影响

靳晓坤[1,2]，徐　乐[1]，尉文超[1]，姚可夫[2]，时　捷[1]，王毛球[1]
(1. 钢铁研究总院 特钢所，北京 100081)
(2. 清华大学 材料学院，北京 100084)

摘　要：研究了未溶和回火析出的(Ti,Mo)C 析出相的氢陷阱作用对调质铬钼钢的超高周疲劳性能的影响。结果表明：球形未溶(Ti,Mo)C 析出相的氢解吸附激活能为 142.6 kJ/mol，这种强氢陷阱在电化学充氢条件下不会捕获氢；细小的回火 (Ti,Mo)C 析出相是有效的氢陷阱，其捕获的氢的解吸附激活能为 17.0 kJ/mol，这部分氢的扩散系数较小，室温放置 336 h 仍不能扩散出试样，但在循环载荷下能够从氢陷阱处解吸附并且向裂纹尖端或应力集中处扩散，仍能在一定程度上降低钢的超高周疲劳强度；位错和晶界处的可逆氢的解吸附激活能为 16.9 kJ/mol，这部分氢扩散系数较大，室温放置 96 h 就能全部扩散出试样，在循环载荷下这部分氢能够迅速向裂纹尖端或应力集中处扩散，显著降低疲劳裂纹扩展应力强度因子门槛值，最终显著降低超高周疲劳强度；考虑到两者捕获的氢含量相当，被细小的回火(Ti,Mo)C 析出相捕获的氢对超高周疲强度的有害作用要远小于位错、晶界处的可扩散氢对超高周疲劳强度的有害作用。非金属夹杂物的氢解吸附激活能为 70.9 kJ/mol，这种强氢陷阱在电化学充氢条件下同样不会捕获氢。

关键词：高强度钢；超高周疲劳；氢；(Ti,Mo)C

作者简介：靳晓坤，男，1987 年生，博士生，钢铁研究总院特钢所，北京 100081，电话：010-62186791，E-mail: 2545835925@qq.com